Contribution from the Department of Chemistry,
The University of Michigan, Ann Arbor, Michigan 48109

Synthesis and Structure of $R_2R^*_2Mo_4S_4$ Cubane Clusters (R, R* = Cp, Cp', Cp*): An Affirmation of the Dahl Binding Model

P. Douglas Williams and M. David Curtis*

Received June 18, 1986

Molybdenum-sulfur cubane clusters of the type $R\text{-}R^*_2Mo_4S_4$ (**1a**, R = C_5H_5, R* = C_5H_4Me; **1b**, R = R* = C_5H_4Me; **1c**, R = C_5H_4Me, R* = C_5Me_5) are readily prepared by the reaction of $R_2Mo_2(SC_3H_6S)_2$ with 2-3 equiv of $R^*_2Mo_2(CO)_4$ (Mo≡Mo). Byproducts are propene and $R^*_2Mo_2(CO)_6$. These $R_4Mo_4S_4$ clusters undergo two, reversible, one-electron oxidations in CH_3CN solvent at potentials in the range -0.1 to -0.2 (0/+1) and -0.8 to -0.9 (+1/+2) V vs. internal Cp_2Fe/Cp_2Fe^+ standard depending on the substituents, R. The structure of **1c** was determined crystallographically: triclinic; a = 10.964 (3), b = 17.910 (5), c = 10.355 (3) Å; α = 106.21 (2), β = 117.38 (2), γ = 85.25 (2)°; V = 1731.4 (9) Å^3; Z = 2; ρ_{calcd} = 1.80, ρ_{obsd} = 1.83 g/cm^3; space group $P2_1$; R = 0.040, R_w = 0.058 based on 3636 reflections with $I \geq 3\sigma(I)$. The structure consists of a tetrahedral Mo_4 core of nearly T_d symmetry with six Mo-Mo distances in the range 2.896-2.905 Å. The μ_3-sulfido ligands cap the triangular faces of the Mo_4 tetrahedron with Mo-S distances in the range 2.33-2.35 Å. The Cp groups are π-bound to the Mo atoms in a normal fashion. The bonding in the clusters $Cp_4M_4X_4$ (M = Cr, Mo; X = O, S) was examined by the EHMO method. The results confirmed the general outlines of a qualitative model previously proposed. The structures and magnetic properties of a variety of $L_nM_4X_4$ cubane clusters are discussed in light of the bonding model.

Introduction

Cubane clusters of the type M_4X_4 (M = transition metal, X = main-group element) are important models of electronic structure in metal clusters. The problem of metal cubane electronic structure has been addressed most extensively by Dahl and co-workers[1] since their initial report of the metal carbonyl cubane $(CO)_{12}Co_4Sb_4$ in 1970.[2] These workers have developed a qualitative molecular orbital (MO) scheme from symmetry arguments[3] and have been able to describe or predict the bonding in a great majority of the cubanes reported. Bottomley and Grein have more recently proposed a different molecular orbital scheme for M_4X_4 cubanes based on extended Hückel molecular orbital (EHMO) calculations.[4] We will discuss these models in light of recently reported results as well as our own EHMO calculations.

We have been interested in rational synthetic routes to novel mixed-metal sulfur clusters and in our studies have found dimers containing the $Cp_2Mo_2S_4$ (Cp = cyclopentadienyl) core to be versatile starting materials.[5] We now report the synthesis and structure of mixed-Cp-ligand Mo_4S_4 cubanes obtained from the reaction of $R_2Mo_2(CO)_4$ (Mo≡Mo) (R = C_5H_4Me(Cp'), C_5Me_5(Cp*)) with the dimers $(RMo(SC_3H_6S))_2$ (R = Cp, Cp').

At the start of this work only scant reference could be found to be the series of cubane clusters $Cp_4M_4S_4$, where M = Cr[6,7] or Mo.[8,9] Comparisons of the structures of the $Cp_4Mo_4S_4$ cubanes with similar compounds, e.g. $(NO)_4Fe_4S_4$ and $(NO)_4Fe_4S_2(N\text{-}t\text{-}Bu)_2$,[10] are useful in testing the validity of symmetry-derived bonding models.[3] Recently, structural determinations of $Cp^*_4Cr_4S_4$[11] and the cubane series $(i\text{-}PrC_5H_4)_4Mo_4S_4^{n+}$ (n = 0-2)[12] have been reported. Also, in a preparation similar to that which we originally reported,[5b] the mixed-Cp, mixed-metal cubanes $Cp_2Cp^*_2M_4S_4$ (M_4 = Cr_4, Cr_2Mo_2, Mo_4) were obtained and characterized, primarily by mass spectrometry.[13]

Experimental Section

All reactions and manipulations were performed under a prepurified nitrogen atmosphere unless noted otherwise. Reagent grade solvents were dried and distilled under nitrogen prior to use. Hexanes were distilled from CaH_2. Dichloromethane was predried over $CaCl_2$ and distilled from P_2O_5. Toluene and THF were distilled from Na/benzophenone. Starting materials were prepared according to published procedures.

NMR spectra were obtained on a Varian T60A instrument. IR spectra were obtained on a Perkin-Elmer 1330 spectrometer. Mass spectra of solid samples were obtained by thermal desorption from the direct inlet of a Finnegan GC-MS. Elemental analyses were obtained from Galbraith (Knoxville, TN) or Schwarzkopf (Woodside, NY) Microanalytical Labs.

Synthesis of $Cp'_2Cp_2Mo_4(\mu_3\text{-}S)_4$ (1a). A mixture of 0.865 g (1.87 mmol) of $Cp'_2Mo_2(CO)_4$[14] and 0.50 g (0.94 mmol) of $[CpMo(\mu\text{-}\eta^2\text{-}SC_3H_6S]_2$[15a] in 40 mL of toluene was heated at 65 °C for 24 h. Cooling of the solution to 0 °C gave the violet powder **1a** upon filtration. IR and NMR spectra of the filtrate showed the only major component to be $Cp'_2Mo_2(CO)_6$. Solid **1a** was recrystallized from CH_2Cl_2/hexane: mp 325 °C; yield 0.20 g (26% based on $[Cp'Mo(\mu\text{-}\eta^2\text{-}SC_3H_6S)]_2$). An attempt to separate the reaction mixture by elution chromatography (Florisil, 50 × 3 cm, CH_2Cl_2) was unsuccessful. Only a single cherry red band ($Cp'_2Mo_2(CO)_6$) eluted, but violet and green bands formed, which could not be eluted from the column.

Synthesis of $Cp'_4Mo_4(\mu_3\text{-}S)_4$ (1b). A. A mixture of 1.23 g (2.67 mmol) of $Cp'_2Mo_2(CO)_4$ and 0.50 g (0.89 mmol) of $[Cp'Mo(\mu\text{-}\eta^2\text{-}SC_3H_5S)]_2$[15a] in 40 mL of toluene was heated at 65 °C for 24 h. Filtration of the cooled mixture gave a slight amount of brown powder, which was discarded. The solvent was removed from the filtrate under vacuum to yield a purple-red solid. This solid was extracted with 25 mL of toluene/hexane (1:2, v/v) to give the violet solid **1b** and a reddish extract, which was shown to contain $Cp'_2Mo_2(CO)_6$ and an unidentified green-brown solid. Compound **1b** obtained from the above procedure was recrystallized from THF/hexane at 0 °C: yield 0.26 g (35% based on $[Cp'Mo(\mu\text{-}\eta^2\text{-}SC_3H_6S)]_2$); mp 215 °C. Anal. Calcd for $Cp'_4Mo_4(\mu_3\text{-}S)_4$ ($C_{24}H_{28}Mo_4S_4$): C, 34.79; H, 3.41; S, 15.48; Mo, 46.32. Found: C, 34.93; H, 3.37; S, 15.60; Mo, 46.36.

B. A mixture of 0.19 g (0.42 mmol) of $Cp'_2Mo_2(CO)_4$ and 0.20 g (0.42 mmol) of $[Cp'Mo(S)(SH)]_2$[5a,15b] in 40 mL of THF was refluxed for 2 h. Removal of solvent left a brown solid from which $Cp'_2Mo_2(CO)_6$ and **1b** could be extracted with toluene/hexane (1:1, v/v). Further purification was not attempted. Yields were obtained from NMR integration of the mixture: 41% $Cp'_2Mo_2(CO)_6$, 37% **1b** (based on $Cp'_2Mo_2(CO)_4$).

(1) Chu, C. T.-W.; Lo, F. Y.-K.; Dahl, L. F. *J. Am. Chem. Soc.* **1982**, *104*, 3409.
(2) Foust, A. S.; Dahl, L. F. *J. Am. Chem. Soc.* **1970**, *92*, 7337.
(3) Trinh-Toan; Teo, B. K.; Ferguson, J. A.; Meyer, T. J.; Dahl, L. F. *J. Am. Chem. Soc.* **1977**, *99*, 408.
(4) Bottomley, F.; Grein, F. *Inorg. Chem.* **1982**, *21*, 4170.
(5) (a) Curtis, M. D.; Williams, P. D. *Inorg. Chem.* **1983**, *22*, 2661. (b) Williams, P. D.; Curtis, M. D.; Duffy, D. N.; Butler, W. M. *Organometallics* **1983**, *2*, 165.
(6) Fischer, E. O.; Ulm, K.; Kuzel, P. *Z. Anorg. Allg. Chem.* **1963**, *319*, 253.
(7) Pasynskii, A. A.; Eremenko, I. L.; Orazsakhatov, B.; Kalinnikov, V. T.; Aleksandrov, G. G.; Struchov, Y. T. *J. Organomet. Chem.* **1981**, *216*, 211.
(8) Dahl, L. F. Presented at the VIth International Conference on Organometallic Chemistry, Amherst, MA, Aug 1973.
(9) Danzer, W. Thesis, Universität München, 1976.
(10) Gall, R. S.; Chu, C. T.-W.; Dahl, L. F. *J. Am. Chem. Soc.* **1974**, *96*, 4019.
(11) Pasynskii, A. A.; Eremenko, I. L.; Rakitin, Y. V.; Novotortsev, V.M.; Ellert, O. G.; Kalinnikov, V. T.; Shklover, V. E.; Struchov, Y. V.; Lindeman, S. V.; Kurbanov, T. K.; Gasanov, G. S. *J. Organomet. Chem.* **1983**, *248*, 309.
(12) Bandy, J. A.; Davies, C. E.; Green, J. C.; Green, M. L. H.; Prout, K.; Rodgers, D. P. S. *J. Chem Soc., Chem. Commun.* **1983**, 1395.
(13) Brunner, H.; Kauermann, H.; Wachter, J. *J. Organomet. Chem.* **1984**, *265*, 189.
(14) Curtis, M. D.; Fotinos, N. A.; Messerle, L.; Sattelberger, A. P. *Inorg. Chem.* **1983**, *22*, 1559.
(15) (a) Rakowski DuBois, M.; Haltiwanger, R. C.; Miller, D. J.; Glatzmaier, G. *J. Am. Chem. Soc.* **1979**, *101*, 5245. (b) Rakowski DuBois, M.; VanDerveer, M. C.; DuBois, D. L.; Haltiwanger, R. C.; Miller, W. K. *Ibid.* **1980**, *102*, 7456.

0020-1669/86/1325-4562$01.50/0

Synthesis of $Cp'_2Cp^*_2Mo_4(\mu_3\text{-}S)_4$ (1c). A 100-mL side-arm flask was filled with 0.49 g (0.87 mmol) of $[Cp'Mo(\mu\text{-}\eta^2\text{-}SC_3H_6S)]_2$, 0.50 g (0.87 mmol) of $Cp^*_2Mo_2(CO)_4$,[14] and 50 mL of toluene. The mxiture was refluxed for 3 h and then reduced to approximately 10 mL total volume in vacuo. Hexane was added to double the volume, and the slurry was transferred to a column of alumina (50 × 2 cm). An initial orange band of unreacted $Cp^*_2Mo_2(CO)_4$ was collected with use of hexane/toluene (2:1, v/v). A purple band followed (hexane/toluene, 1:1), yielding dark purple crystals of **1c**, which were recrystallized from CH_2Cl_2/hexane: yield 0.35 g (43%); mp >350 °C. Anal. Calcd for $Cp'_2Cp^*_2Mo_4(\mu\text{-}S)_4$ ($C_{32}H_{44}Mo_4S_4$): C, 40.86; H, 4.71; Mo, 40.80; S, 13.63. Found: C, 40.70; H, 4.65; Mo, 40.61; S, 13.69.

A final green band was collected from the chromatography column (toluene/THF, 3:1), yielding an air-sensitive, oily, green solid (**2**), which was recrystallized from CH_2Cl_2/hexane: yield 0.20 g; mp 135–145 °C. Anal. Found: C, 37.04; H, 4.30; Mo, 38.95; S, 19.87. This suggests the composition $Mo_2S_3C_{15}H_{21}$. Anal. Calcd: C, 36.81; H, 4.32; Mo, 39.21; S, 19.65.

Reaction of $Cp_2W_2(CO)_4$ and $[Cp'Mo(\mu\text{-}\eta^2\text{-}SC_3H_6S)_2]_2$. A toluene solution containing equimolar concentrations of these two reactants was refluxed for 2 h, during which time the color changed from orange to purple-brown. Crystallization and chromatography gave $Cp_2W_2(cO)_6$ and unidentified, impure purple and brown solids.

Description of the Cyclic Voltammetry Experiments. The apparatus for cyclic voltammetry has been described elsewhere.[16] All experiments employed a Pt-wire working electrode in 0.10 M Et_4NBF_4 in acetonitrile referenced to a 0.01 M Ag^+/Ag cell. The sample cell included a 0.001 M concentration of the cluster of interest (or less, depending on solubility). Scan rates were between 50 and 200 mV/s. Acetonitrile was purified by allowing it to stand over CaH_2 for several days followed by distillation from CaH_2, fractional distillation from P_2O_5 (81–82 °C collected), and, finally, distillation again from CaH_2 just prior to use. Tetraethylammonium tetrafluoroborate was dried in vacuo (0.1 mmHg) at 110 °C for 6 h and stored under N_2 until used. The ferrocene/ferrocenium redox couple was used as an internal standard to reference the system to other work.[17]

X-ray Structure Determination of $Cp'_2Cp^*_2Mo_4(\mu_3\text{-}S)_4$ (1c). Single crystals of **1c** were obtained by slow cooling of a saturated hexane solution to −20 °C. X-ray data were collected[18] and heavy atoms were located with use of MULTAN[19] assisted by input of a Mo_4 tetrahedron (bond distances obtained from a Patterson maps. The remaining atoms were located in subsequent difference maps. Some of the C–C distances were unreasonable, and the thermal parameters of several methyl carbons were large. An attempt was made to model the cyclopentadienes attached to Mo3 and Mo4 by insertion of two complementary, coplanar rings, related to each other by a 36° rotation about the Mo–centroid axis. Parameters for this model refined poorly, however, and the model was discarded. The possibility of a Cp′/Cp* site occupancy disorder was considered but could not be detected in any of the difference maps. All non-hydrogen atoms were refined to anisotropic convergence. Refinement minimized the function $\sum w(|F_o| - |F_c|)^2$, where $|F_o|$ and $|F_c|$ were the observed and calculated structure factor amplitudes. The weighting factors w were taken as $w = 4F_o^2/(\sigma^2(F_o^2) + (PF_o^2)^2)$, where P, the factor to prevent overweighting of strong reflections, was set equal to 0.04. The agreement indices $R_1 = \sum||F_o| - |F_c||/\sum|F_o|$ and $R_2 = (\sum w(|F_o| \text{ in } |F_c|)^2/\sum wF_o^2)^{1/2}$ were used to evaluate the refinement. An absorption correction[20] was applied to the data after all the atoms were found.

(16) (a) Rasmussen, P. G.; Anderson, J. E.; Bayon, J. C. *Inorg. Chim. Acta* **1984**, *87*, 159. (b) Bailey, O. H. Ph.D. Thesis, The University of Michigan, Ann Arbor, MI, 1983.
(17) Gritzner, G.; Kuta, J. *Pure Appl. Chem.* **1982**, *54*, 1527.
(18) A Syntex $P2_1$ four-circle diffractometer was employed for X-ray analysis. Crystal lattice parameters were determined from a least-squares refinement of 15 reflection settings obtained from an automatic centering routine. Intensity data were obtained at 22 °C with use of Mo Kα radiation monochromatized (0.71069 Å) by a graphite crystal. Three standard reflections were measured every 50 reflections.
(19) Direct methods program MULTAN78 by Peter Main.
(20) Computations were carried out on an Amdahl 470/V7 computer at the University of Michigan Computing Center. Programs used during the structure analysis were SYNCOR (data reduction by W. Shmonsees), FORDAP (Fourier synthesis by A. Zalkin), ORFLS (full-matrix least-squares refinement by Busing, Martin, and Levy), ORFFE (distances and angles and their esd's by Busing, Martin, and Levy), and ORTEP (thermal ellipsoid plots by C. K. Johnson). ABSORB (absorption correction by D. Templeton and L. Templeton), HFINDR (calculation of hydrogen positions by A. Zalkin), and PLANES (calculation of least-squares planes by D. M. Blow) were used in some cases as specified in the text. The atom scattering factors used were obtained from: *International Tables for X-ray Crystallography*; Kynoch: Birmingham, England, 1974; Vol. IV, Tables 2.2 and 2.3.1.

Table I. Summary of Crystal and Data Statistics for $Cp'_2Cp^*_2Mo_4(\mu_3\text{-}S)_4$ (1c)

color	violet
chem formula	$C_{32}H_{44}Mo_4S_4$
mol wt	940.70
space group	$P\bar{1}$
a, b, and c, Å	10.964 (3), 17.910 (5), 10.355 (3)
α, β, γ, deg	106.21 (2), 117.38 (2), 85.25 (2)
V, Å^3	1731.4 (9)
Z	2
ρ_{calcd}, g/cm^3	1.80
ρ_{obsd}, g/cm^3	1.83 (flotation)
cryst dimens, mm	0.225 × 0.237 × 0.220
μ(Mo Kα), cm^{-1}	16.37
scan speed, deg/min	2.5–12, variable
scan range, deg	Mo $K\alpha_1$ − 0.8 to Mo $K\alpha_2$ + 0.9
bkgd/scan time	0.8
2θ, deg	45
reflecns measd	$+h,\pm k,\pm l$
no. of reflecns	4849 (3636 with $I \geq 3\sigma(I)$)
N_o/N_v	10.1
goodness of fit	2.01
R_1, R_2	0.040, 0.058
residual, e/Å^3	0.97
largest shift/error on final cycle	1.65

Table II. Atomic Positions for $Cp'_2Cp^*_2Mo_4(\mu_3\text{-}S)_4$ (1c)

atom	x	y	z
Mo1	0.1698 (1)	0.2943 (1)	0.1865 (1)
Mo2	0.2281 (1)	0.3395 (1)	−0.0290 (1)
Mo3	0.2390 (1)	0.1777 (1)	−0.0243 (1)
Mo4	−0.0234 (1)	0.2500 (1)	−0.1320 (1)
S1	0.1334 (3)	0.2289 (1)	−0.2327 (3)
S2	0.0598 (2)	0.1727 (1)	0.0356 (3)
S3	0.0477 (2)	0.3748 (1)	0.0323 (3)
S4	0.3757 (2)	0.2847 (1)	0.1674 (2)
C1	0.271 (1)	0.282 (1)	0.435 (1)
C2	0.123 (1)	0.270 (1)	0.372 (1)
C3	0.067 (1)	0.343 (1)	0.343 (1)
C4	0.174 (1)	0.396 (1)	0.391 (1)
C5	0.296 (1)	0.358 (1)	0.447 (1)
CA	0.378 (2)	0.224 (1)	0.493 (1)
CB	0.050 (2)	0.196 (1)	0.357 (1)
CC	−0.086 (1)	0.361 (1)	0.283 (2)
CD	0.155 (2)	0.482 (1)	0.390 (2)
CE	0.437 (1)	0.399 (1)	0.518 (1)
C6	0.425 (1)	0.413 (1)	0.024 (2)
C7	0.355 (2)	0.375 (1)	−0.136 (2)
C8	0.222 (2)	0.406 (1)	−0.199 (2)
C9	0.209 (1)	0.462 (1)	−0.076 (2)
C10	0.332 (1)	0.465 (1)	0.061 (1)
CF	0.570 (1)	0.403 (1)	0.122 (2)
C11	0.422 (2)	0.111 (1)	−0.053 (3)
C12	0.416 (2)	0.096 (1)	0.073 (2)
C13	0.297 (2)	0.055 (1)	0.014 (2)
C14	0.229 (2)	0.044 (1)	−0.133 (2)
C15	0.289 (2)	0.073 (1)	−0.181 (2)
CG	0.528 (2)	0.154 (1)	−0.072 (4)
CH	0.526 (3)	0.113 (1)	0.221 (2)
CI	0.227 (3)	0.010 (1)	0.077 (4)
CJ	0.087 (2)	−0.001 (1)	−0.256 (3)
CK	0.270 (4)	0.074 (2)	−0.340 (2)
C16	−0.210 (1)	0.264 (1)	−0.351 (2)
C17	−0.240 (1)	0.297 (1)	−0.228 (2)
C18	−0.252 (2)	0.243 (2)	−0.179 (2)
C19	−0.220 (2)	0.158 (2)	−0.274 (3)
C20	−0.202 (2)	0.185 (1)	−0.364 (2)
CL	−0.191 (3)	0.312 (2)	−0.438 (3)

Hydrogen atoms were not located.

Crystal and data statistics are given in Table I. Final positional and thermal parameters with estimated standard deviations are given in Tables II and III, respectively (Table III is given in the supplementary material).

Results and Discussion

Synthesis and Characterization of $R_4Mo_4S_4$ Clusters. The isolobal relationship between the triply bonded compounds Cp-

Table IV. Spectroscopic Data for the Mo_4S_4 Clusters

compd	^{1}H NMR, δ	λ_{max}, nm (ϵ, 10^{-3} M^{-1} cm^{-1})	mass spec, m/e
$(MeCp)_2Cp_2Mo_4S_4$ (**1a**)	2.02 (s, 6 H), 5.12 (m, 8 H), 5.17 (s, 10 H) ($CDCl_3$)		800 (P^+) 785 ($P^+ - CH_3$), 721 ($P^+ -$ MeCp), 400 (P^{2+})
$(MeCp)_4Mo_4S_4$ (**1b**)	2.05 (s, 12 H), 5.12 (2 m, 16 H) (C_6D_6)	520 (2.8)	828 (P^+), 813 ($P^+ - CH_3$), 749 ($P^+ -$ MeCp), 670 ($P^+ - 2$MeCp), 414 (P^{2+})
$(MeCp)_2(Me_5Cp)_2Mo_4S_4$ (**1c**)	2.03 (s, 30 H), 2.13 (s, 6 H), 4.97 (2 m, 8 H) (C_6D_6)	530 (3.3)	940 (P^+), 470 (P^{2+})

Table V. Cyclic Voltammetric Data for Mo_4S_4 Cubane Clusters

compd	$E_{p/2}$, V	ΔE_p, mV	i_{pc}/i_{pa}	$E'_{p/2}$, V[d]
$(MeCp)_4Mo_4S_4$ (**1b**)	−0.82[a]	60	1.0	−0.89
	−0.12	60	0.9	−0.19
$(i\text{-}PrCp)_4Mo_4S_4$	−0.33[b]	60	1.0	−0.76
	+0.32	60	1.0	−0.11
$Cp_2(Me_5Cp)_2Mo_4S_4$	−0.63[c]			
	+0.11			

[a] Conditions: vs. Ag/Ag^+; $E_{p/2}(Fc/Fc^+)$ = +0.07 V; 0.10 M Et_4NBF_4 in CH_3CN (this work). [b] Conditions: vs. SCE; $E_{p/2}(Fc/Fc^+)$ = +0.43 V; 0.1 M Et_4NClO_4 in DMF.[12] [c] Conditions: vs. SCE; no internal standard reported; 0.10 M Bu_4NClO_4 in CH_4CN; ΔE_p and current ratios not reported; both waves reported to be reversible.[13] [d] Vs. reported Fc/Fc^+ internal standard.

$(CO)_2Mo{\equiv}Mo(CO)_2Cp$[21] and HC≡CH was used to design the synthesis of Mo_4S_4 cubanes (**1**). DuBois et al. had shown that $[CpMo(SC_3H_6S)_2]_2$ reacts with HC≡CH to form $[CpMo(SC_2H_2S)_2]_2$ and propene (eq 1).[15a,22] Substitution of C≡C with

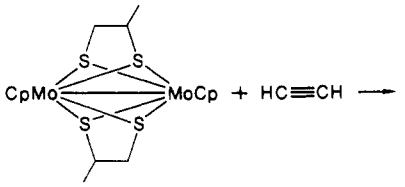

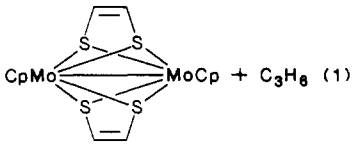

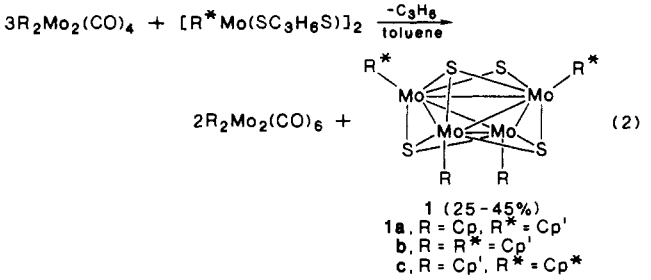

M≡M also results in displacement of propene and the formation of cubane clusters of the type $R_4Mo_4S_4$. The reaction shown in eq 2 occurs in refluxing toluene. Two or three equivalents of $R_2Mo_2(CO)_4$ (R = Cp', Cp*) per equivalent of $[R'Mo(\mu\text{-}\eta^2\text{-}SC_3H_6S)]_2$ (R' = Cp, Cp') results in formation of the cubane clusters **1a–c** in moderate yields. Excess triply bonded carbonyl is used since the evolved CO converts the tetracarbonyl dimer to the unreactive singly bonded hexacarbonyl dimer. Spectroscopic data for the cubane clusters are given in Table IV. Cluster **1b** was also obtained but not isolated from the reaction of

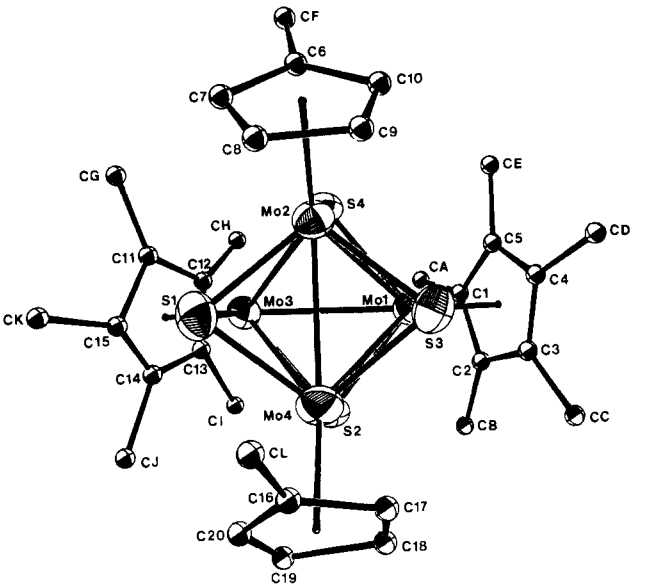

Figure 1. ORTEP plot of $Cp'_2Cp^*_2Mo_4(\mu_3\text{-}S)_4$ (**1c**). Carbon thermal factors are set artificially low for illustration. The remaining thermal ellipsoids are drawn at the 50% probability level.

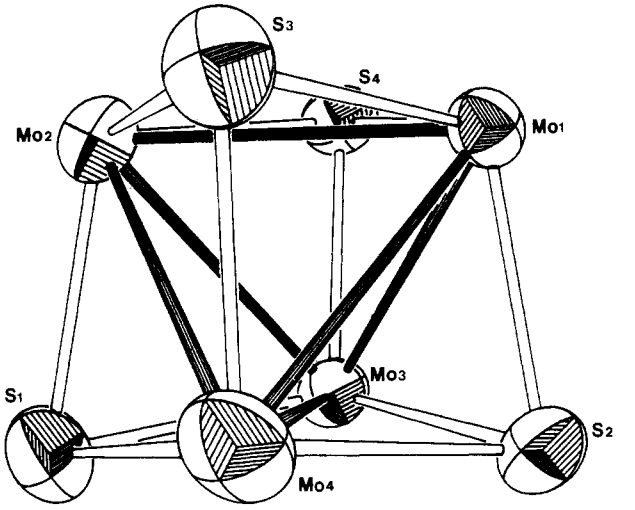

Figure 2. Cluster core of $Cp'_2Cp^*_2Mo_4(\mu_3\text{-}S)_4$ (**1c**). Thermal ellipsoids are drawn at the 50% probability level.

$[Cp'Mo(\mu\text{-}S)(\mu\text{-}SH)]_2$ with $Cp'_4Mo_2(CO)_4$.

A green compound (**2**) was obtained as a byproduct in all these syntheses. Mass spectral, IR, and NMR data indicatd the green compounds were probably paramagnetic $R_nR'_{3-n}Mo_3S_4$ clusters,[13,23,24] but these were not purified or definitely identified.

An attempt to prepare the mixed-Mo_2W_2 cubane cluster from $Cp_2W_2(CO)_4$ and $[Cp'Mo(\mu\text{-}\eta^2\text{-}SC_3H_6S)]_2$ yielded $Cp_2W_2(CO)_6$ and two other products in low yield, the NMR spectra of which

(21) (a) Curtis, M. D.; Messerle, L.; Fotinos, N. A.; Gerlach, R. F. In *Reactivity of Metal-Metal Bonds*; ACS Symposium Series 155; Chisholm, M. H., Ed.; American Chemical Society: Washington, D.C, 1981; pp 221–258. (b) Curtis, M. D. *Polyhedron*, in press.
(22) DuBois, D. L.; Miller, W. K.; Rakowski DuBois, M. *J. Am. Chem. Soc.* **1981**, *103*, 3429.
(23) Vergamini, P. J.; Vahrenkamp, H.; Dahl, L. F. *J. Am. Chem. Soc.* **1971**, *93*, 6327.
(24) (a) Danzer, W.; Fehlhammer, W. P.; Liu, A. T.; Thiel, G.; Beck, W. *Chem. Ber.* **1982**, *115*, 1682. (b) Beck, W.; Danzer, W.; Thiel, G. *Angew. Chem., Int. Ed. Engl.* **1973**, *12*, 582.

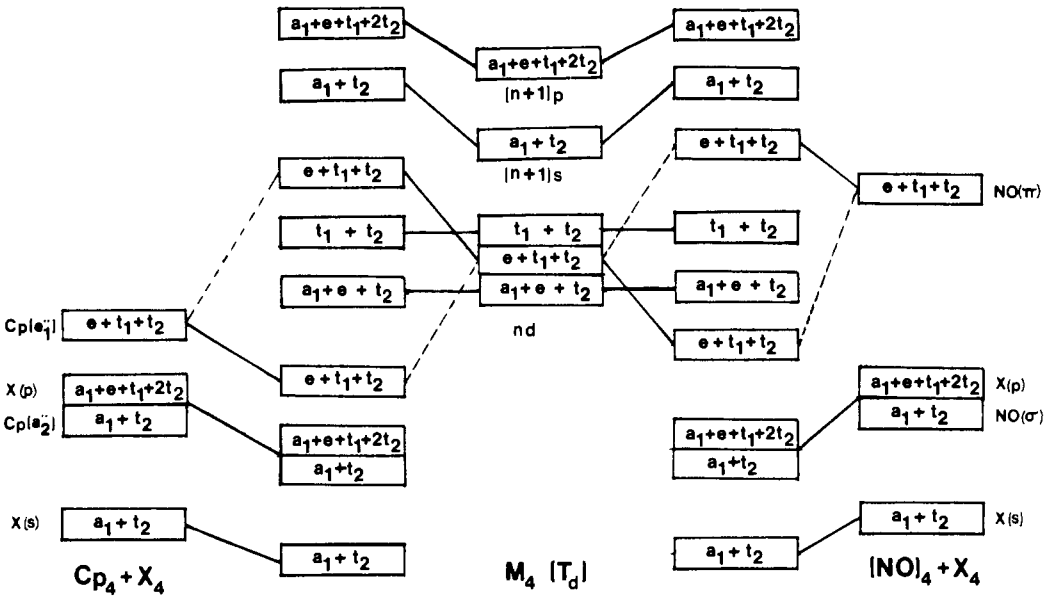

Figure 3. Qualitative interaction scheme according to the Dahl model.

Table VI. Distances (Å) for $(MeCp)_2(Me_5Cp)_2Mo_4(\mu_3\text{-}S)_4$ (**1c**)

	Cluster Core		
Mo1–Mo2	2.906 (1)	Mo1–Mo3	2.902 (1)
Mo1–Mo4	2.896 (2)	Mo2–Mo3	2.904 (1)
Mo2–Mo4	2.896 (1)	Mo3–Mo4	2.905 (1)
Mo1–S2	2.333 (2)	Mo1–S3	2.327 (2)
Mo1–S4	2.343 (2)	Mo2–S1	2.334 (3)
Mo2–S3	2.332 (2)	Mo2–S4	2.354 (2)
Mo3–S1	2.339 (2)	Mo3–S2	2.331 (2)
Mo3–S4	2.340 (2)	Mo4–S1	2.347 (3)
Mo4–S2	2.331 (3)	Mo4–S3	2.333 (3)
S1–S2	3.625 (5)	S3–S4	3.628 (4)
S1–S3	3.634 (5)	S2–S4	3.627 (4)
S1–S4	3.637 (4)	S2–S3	3.620 (4)
	Metal–Ligand[a]		
Mo1–C1	2.36 (1)	Mo1–C2	2.36 (1)
Mo1–C3	2.32 (1)	Mo1–C4	2.36 (1)
Mo1–C5	2.37 (1)	Mo1–CT1	2.02
Mo2–C6	2.39 (1)	Mo2–C7	2.35 (1)
Mo2–C8	2.36 (1)	Mo2–C9	2.34 (1)
Mo2–C10	2.34 (1)	Mo2–CT2	2.01
Mo3–C11	2.34 (1)	Mo3–C12	2.35 (1)
Mo3–C13	2.33 (1)	Mo3–C14	2.32 (1)
Mo3–C15	2.32 (1)	Mo3–CT3	2.03
Mo4–C16	2.31 (1)	Mo4–C17	2.30 (1)
Mo4–C18	2.33 (2)	Mo4–C19	2.41 (2)
Mo4–C20	2.34 (1)	Mo4–CT4	2.02
	Intraligand		
C1–C2	1.45 (2)	C1–C5	1.38 (1)
C1–CA	1.51 (2)	C2–C3	1.44 (2)
C2–CB	1.54 (2)	C3–C4	1.38 (2)
C3–CC	1.55 (2)	C4–C5	1.39 (2)
C4–CD	1.55 (2)	C5–CE	1.51 (2)
C6–C7	1.44 (2)	C6–C10	1.44 (2)
C6–CF	1.47 (2)	C7–C8	1.43 (2)
C8–C9	1.44 (2)	C9–C10	1.43 (2)
C11–C12	1.43 (2)	C11–C15	1.49 (2)
C11–CG	1.57 (2)	C12–C13	1.34 (2)
C12–CH	1.41 (2)	C13–C14	1.31 (2)
C13–CI	1.59 (2)	C14–C15	1.20 (2)
C14–CJ	1.59 (2)	C15–CK	1.58 (2)
C16–C17	1.41 (2)	C16–C20	1.38 (2)
C16–CL	1.50 (2)	C17–C18	1.25 (3)
C18–C19	1.67 (4)	C19–C20	1.26 (3)

[a] CT = MeCp and Me_5Cp centroids.

indicated neither to be a heteronuclear cluster.

Cyclic voltammetric (CV) data for cubanes are compared in Table V. Both **1b** and the $i\text{-}PrC_5H_4$ derivative undergo two successive and reversible one-electron oxidations with **1b** being easier (ca. 0.1 V) to oxidize. No reduction processes for these cubanes are observed at $E > -2.5$ V vs. Ag/Ag^+. However, $Cp_2Cp^*_2Mo_4S_4$ has been reported to undergo reversible one-electron *reduction* (−0.63 V) and oxidation (+0.11 V).[13] Since the difference of these $E_{p/2}$ values is similar to those for **1b** and $(i\text{-}PrC_5H_4)_4Mo_4S_4$, it is likely that the so-called reduction wave has been misinterpreted and is actually the 0/+1 oxidation wave.

Structure of $Cp'_2Cp^*_2Mo_4S_4$ (1c). The structure of **1c** was determined by X-ray diffraction. Listings of the atomic distances and selected angles for **1c** are given in Tables VI and VII. ORTEP plots of the molecule are shown with and without ligands in Figures 1 and 2, respectively.

The Mo_4 core displays nearly regular T_d symmetry (Mo–Mo = 2.896–2.905 Å) although there is no crystallographically imposed symmetry. The μ_3-sulfido ligands symmetrically cap the faces of the Mo_4 tetrahedron (S···S = 3.620–3.637 Å) and preserve the high symmetry. The Mo–Mo bond lengths are in the range observed in other compounds in which a Mo–Mo single bond is bridged by two sulfide ligands.[25]

It is clear from the intraring distances and angles that several atoms, particularly C14, C18, and C19, are poorly located. Various attempts to model librational disorder in the rings gave no better results and were discarded. The metal–ring centroid distances all lie in the range 2.01–2.03 Å; thus, no significant differences in the bonding of the Cp′ and Cp* rings to Mo are discerned. The average value for the three CT–Mo–Mo′ (CT = ring centroid) angles about each Mo is very nearly 144.7° for all of the four Mo atoms. Individual angles are observed to deviate up to ±1.9° from the mean value, but the deviations do not occur in a manner which can be related to the steric bulk of the Cp* rings.

The Mo_4S_4 core of $(i\text{-}PrC_5H_4)_4Mo_4S_4$[12] is nearly identical with that in **1c**. The Cr_4S_4 core of $Cp'_4Cr_4S_4$ also has nearly regular T_d symmetry although the range of the Cr–Cr distances (2.822–2.848 Å) is slightly larger than that of the Mo–Mo distances in the Mo_4S_4 cubanes.[11] Tetrahedral symmetry, in fact, seems to be typical for these cubanes, which contain 60 valence shell electrons (VSE; sulfur ligands counted as 4-electron donors). Other similarly described 60-VSE M_4X_4 clusters include $(CN)_{12}Mo_4S_4^{8-}$,[26] $(NO)_4Fe_4S_4$,[1,10] and $Cp_4Fe_4(\mu_3\text{-}CO)_4$.[27] The only such cluster to deviate significantly from T_d symmetry is

(25) Curtis, M. D.; Williams, P. D., to be submitted for publication.
(26) Müller, A.; Eltzner, W.; Bögge, H.; Jostes, R. *Angew. Chem., Int. Ed. Engl.* **1982**, *21*, 795.
(27) Neuman, M. A.; Trinh-Toan; Dahl, L. F. *J. Am. Chem. Soc.* **1972**, *94*, 3383.

Table VII. Angles (deg) about Core Atoms[a] for $Cp'_2Cp^*_2Mo_4(\mu_3\text{-}S)_4$ (1c)

Mo2″-Mo1-Mo3	60.00 (3)	Mo2-Mo1-Mo4	59.87 (4)
Mo3-Mo1-Mo4	60.14 (3)	S2-Mo1-Mo3	51.49 (6)
S2-Mo1-Mo4	51.60 (7)	S3-Mo1-Mo2	51.48 (6)
S3-Mo1-Mo4	51.67 (7)	S4-Mo1-Mo2	51.95 (6)
S4-Mo1-Mo3	51.66 (6)	CT1-Mo1-Mo2	144.1
CT1-Mo1-Mo3	146.0	CT1-Mo1-Mo4	144.1
Mo1-Mo2-Mo3	59.92 (3)	Mo1-Mo2-Mo4	59.88 (3)
Mo3-Mo2-Mo4	60.11 (3)	S1-Mo2-Mo3	51.66 (6)
S1-Mo2-Mo4	51.99 (7)	S3-Mo2-Mo1	51.33 (6)
S3-Mo2-Mo4	51.65 (7)	S4-Mo2-Mo1	51.60 (6)
S4-Mo2-Mo3	51.56 (6)	CT2-Mo2-Mo1	145.2
CT2-Mo2-Mo3	145.5	CT2-Mo2-Mo4	143.4
Mo1-Mo3-Mo2	60.08 (3)	Mo1-Mo3-Mo4	59.83 (3)
Mo2-Mo3-Mo4	59.80 (3)	S1-Mo3-Mo2	51.49 (7)
S1-Mo3-Mo4	51.82 (7)	S2-Mo3-Mo1	51.56 (6)
S2-Mo3-Mo4	51.47 (7)	S4-Mo3-Mo1	51.75 (6)
S4-Mo3-Mo2	52.00 (6)	CT3-Mo3-Mo1	144.9
CT3-Mo3-Mo2	146.2	CT3-Mo3-Mo4	143.2
Mo1-Mo4-Mo2	60.24 (3)	Mo1-Mo4-Mo3	60.03 (3)
Mo2-Mo4-Mo3	60.09 (3)	S1-Mo4-Mo2	51.58 (7)
S1-Mo4-Mo3	51.57 (6)	S2-Mo4-Mo1	51.65 (6)
S2-Mo4-Mo3	51.45 (6)	S3-Mo4-Mo1	51.49 (6)
S3-Mo4-Mo2	51.61 (6)	CT4-Mo4-Mo1	143.7
CT4-Mo4-Mo2	146.6	CT4-Mo4-Mo3	143.7
Mo2-S1-Mo3	76.85 (8)	Mo2-S1-Mo4	76.43 (8)
Mo3-S1-Mo4	76.61 (8)	Mo1-S2-Mo3	76.95 (8)
Mo1-S2-Mo4	76.76 (8)	Mo3-S2-Mo4	77.08 (8)
Mo1-S3-Mo2	77.19 (8)	Mo1-S3-Mo4	76.84 (8)
Mo2-S3-Mo4	76.74 (8)	Mo1-S4-Mo2	76.45 (7)
Mo1-S4-Mo3	76.59 (7)	Mo2-S4-Mo3	76.44 (7)

[a] CT = MeCp and Me_5Cp centroids.

$Cp_4Cr_4O_4$,[28], which displays a mild distortion to D_2 symmetry although the Cr–Cr contacts all remain within acceptable bonding distance (2 × 2.707, 2 × 2.826, 2 × 2.898 Å).

Qualitative MO Models for Cubane Clusters. The qualitative interaction diagram for a cubane with T_d symmetry is illustrated in Figure 3 according to Dahl et al.[1,3] The 20 *n*d orbitls of an M_4 fragment transform into M–M bonding ($a_1 + e + t_2$), nonbonding ($e + t_1 + t_2$), and antibonding ($t_1 + t_2$) sets. The higher lying ($n + 1$)s and p orbitals transform as $a_1 + t_2$ and $a_1 + e + t_1 + 2t_2$ sets, respectively. Interaction of the M_4 fragment with the $(\mu_3\text{-}X)_4L_4$ ligand sphere is shown to occur in two ways, depending on whether L is a π acid (NO) or π donor (Cp). In either case, the μ_3-X capping atom donates a set of filled p orbitals, which are represented as $a_1 + e + t_1 + 2t_2$. The lowest lying orbitals on X (mostly s character) transform as $a_1 + t_2$ and interact only weakly with the M_4 fragment. The ligands L each supply three orbitals with σ and π symmetry with respect to the M–L axis. The orbitals of σ symmetry are lower in energy and transform as $a_1 + t_2$, while the higher lying π types yield an $e + t_1 + t_2$ set.

For both acceptor and donor ligands, the L(σ) and X(p) sets interact strongly with the ($n + 1$)s and p orbitals on the M_4 fragment to form corresponding bonding and antibonding orbitals. However, the interaction between the M_4 and ligand $e + t_1 + t_2$ sets depends on the nature of the ligand. In the case where L = Cp, the interaction results in a stabilized $e + t_1 + t_2$ set that is primarily ligand-centered. When L = NO, the result is a metal-centered orbital set that is stabilized by M–L π back-bonding. The important feature in both cases is that the $e + t_1 + t_2$ M–M nonbonding set (predisposed for M–L bonding) is removed from the frontier orbital region. Thus, as far as number and types of molecular orbitals are concerned, both types of ligand yield the same qualitative result and should be applicable to systems having the M_4X_4 cubane core but having a variety of terminal ligands. The main criterion for the applicability of the qualitative scheme is that each terminal ligand use three orbitals to bind to the metal. Whether these orbitals are of the σ-donor, π-donor, or π-acceptor type is not important to the general features of the model.

The frontier region of the Dahl orbital scheme consists of six M–M bonding orbtials ($a_1 + e + t_2$) and six antibonding orbitals ($t_1 + t_2$). This group of frontier orbitals is formally nonbonding with respect to the L- or X-centered orbitals.

Valence electron counts are then derived as follows. The $a_1 + t_2$ s orbitals (or lone pairs) of the capping atoms, X, require 8 electrons. These electrons are not considered in the VSE count. The 24 M–L bonding orbitals require 48 electrons, which fill all orbitals up through the $e + t_1 + t_2$ block. Valence electrons in excess of 48 occupy the M–M-centered frontier orbitals.

Some relevant properties of structurally characterized homonuclear M_4X_4 clusters are listed in Table VIII. Homonuclear clusters are here defined to contain only one type each of metal (M) and capping atom (X). The compounds in Table VIII are arranged according to the number of valence electrons present in each cluster in *excess* of those necessary for metal–ligand bonding.

An excess of 12 electrons (60 VSE total) completely fills the $a_1 + e + t_2$ M–M bonding set, giving 6 M–M bonds. A regular tetrahedral structure is therefore expected (and observed) for all 12-electron clusters in Table VIII with the exception of $Cp_4Cr_4O_4$. An excess electron count of 24 fills the antibonding $t_1 + t_2$ set so that all M–M bonding is canceled. Note that all of the cubanes in Table VIII with terminal CO ligands have 24 excess electrons. In an $M_4X_4(CO)_{12}$ cubane with CO σ-donor orbitals transform in the same way as the Cp orbitals in Figure 3. However, the CO ligands π back-bond to the M_4 core and stabilize the M–M bonding and antibonding orbitals. Stabilization of these orbitals favors their complete occupation; thus, a 24-electron count is observed for nearly all of the carbonyl cubanes.[29]

Formal M–M bond orders consistent with partial filling of the M–M antibonding orbitals are shown in Table VIII. Most of these clusters display distortions from T_d symmetry according to first-order Jahn–Teller effects, which result from the partial filling of the degenerate orbitals in the M–M antibonding set. These distortions have been discussed in a series of elegant papers by Dahl and co-workers (see references listed in Table VIII).

The clusters with less than 12 excess electrons fall into 2 groups: those with Cp-type ligands and those with N-, O- and S-containing ligands. The latter group of cubanes exhibits D_{2d} symmetry and bond lengths that are consistent with the bond orders derived from the qualitative Dahl model. In each of these clusters, the ligand sphere symmetry is also D_{2d} and probably stabilizes this particular distortion of the M_4X_4 core.

The Cp-substituted cubanes with less than 12 excess electrons show only slight, irregular distortions from T_d symmetry as well as a general *contraction* of the M–M bonds as electrons are removed. These effects are *not* predicted by the qualitative Dahl model since depopulation of the M–M bonding orbitals should cause bond lengthening.

EHMO Calculations for M_4X_4 Cubane Clusters. Recently, another model for bonding in M_4X_4 cubanes was proposed by Bottomley and Grein (BG).[4] This model, based on extended Hückel type calculations for a variety of cubane clusters, arranges the 12 M–M frontier orbitals in order of increasing energy, $e < 1t_2 < t_1 < 2t_2 < a_1$. This order differs primarily from the Dahl model in placing the a_1 orbital at relatively high energy.

Bottomley and Grein also calculated the effect on the total energy of various distortions of the cubane from T_d to D_{2d} or D_2 symmetries. Their results predict that the T_d geometry is less stable than D_2 or D_{2d} for *any* of the electron counts considered here. (The BG model predicts a $^3T_1$ state for 12 excess electrons in a T_d symmetry cubane cluster. This degenerate state is unstable with respect to a first-order Jahn–Teller distortion.) The data in Table VIII show, however, that the T_d geometry is clearly favored for clusters with 12 and 24 excess electrons. Thus, the experimental data appear to be more in harmony with the qualitative Dahl model than with the EHMO-based BG model.

(28) Bottomley, F.; Paez, D. E.; White, P. S. *J. Am. Chem. Soc.* **1982**, *104*, 5651.

(29) Cationic derivatives of $(CO)_{12}Fe_4X_4$ (X = S, Se) with 23 excess electrons have been prepared from oxidation with Br_2 or ICl.[58]

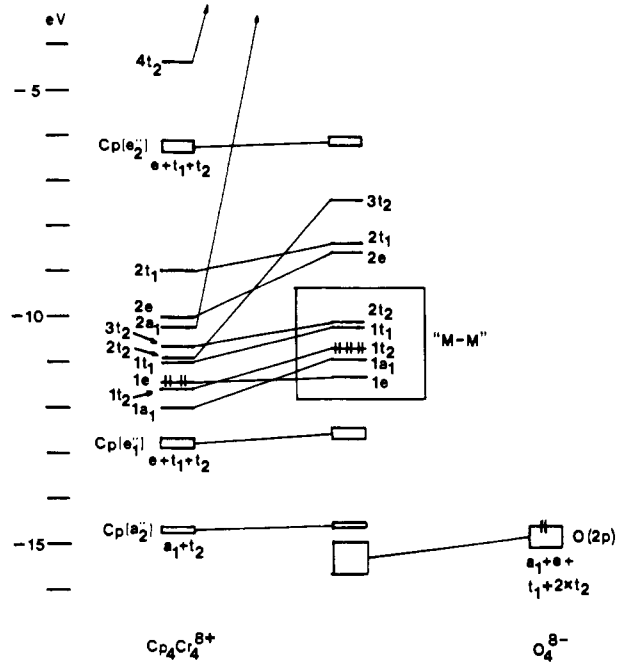

Figure 4. FMO interaction diagram for $Cp_4Cr_4O_4$.

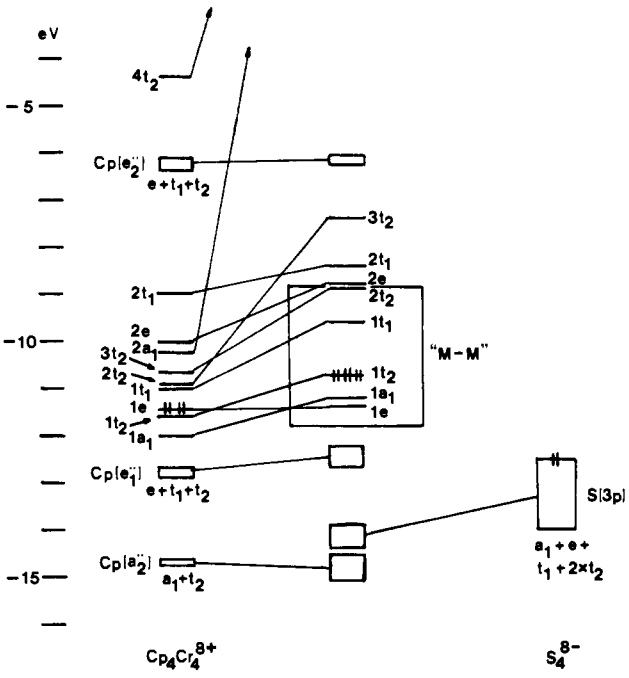

Figure 5. FMO interaction diagram for $Cp_4Cr_4S_4$.

To gain more insight into the electronic structures of these clusters, we have performed EHMO calculations for the clusters $Cp_4M_4X_4$ (M = Cr, Mo; X = O, S) with the "standard" parameters of Hoffmann and co-workers (see Appendix). The clusters were treated as Cp_4M_4 and X_4 fragments in order to ascertain the effects of the M–X interactions, suggested by BG[4] to be important in raising the energy of the a_1 frontier orbital (see above).

The geometry of the M_4X_4 core was idealized to T_d symmetry (strict D_{2d} with Cp rings). The coordinate system is as shown:

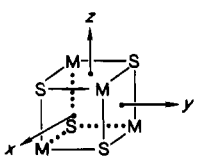

Figures 4 and 5 show the interactions between the Cp_4Cr_4 and X_4 fragments in the $Cp_4Cr_4O_4$ and $Cp_4Cr_4S_4$ clusters, respectively. The orbitals are labeled according to idealized T_d symmetry. Few significant differences between the Cr and Mo clusters emerged from the calculations. Therefore, we will refer mainly to the Cr results to illustrate the conclusions.

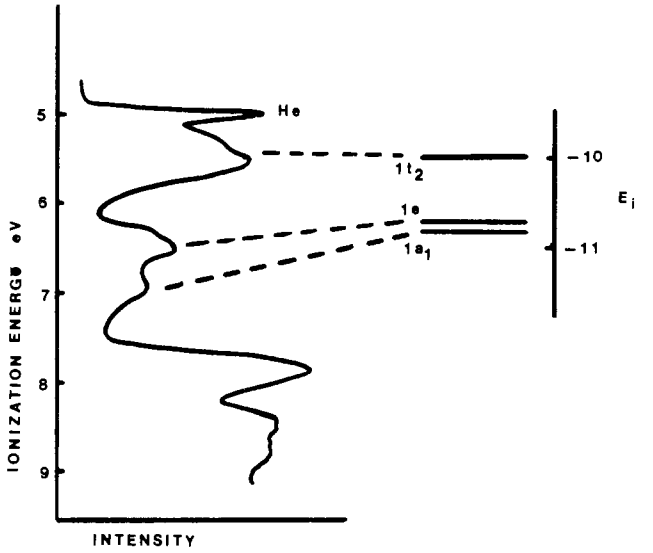

Figure 6. Photoelectron spectrum (adapted from ref 12) compared to the calculated energies of the $1a_1$, 1e, and $1t_2$ orbitals of $Cp_4Mo_4S_4$ on the right.

The X_4^{8-} fragments have two blocks of fragment molecular orbitals (FMO's) well-separated in energy. These blocks are composed of $a_1 + t_2$ sets at low energy (ca. −32 and −20 eV for X = O, S, respectively) arising from interactions of the s orbitals on the X atoms. The higher lying block $a_1 + e + t_1 + 2t_2$ is mostly p character and contains the orbitals that interact most strongly with the $Cp_4Cr_4^{8+}$ FMO's. The O_4^{8-} orbital blocks are more compact in energy than those of S_4^{8-} due to the smaller atomic orbitals and, consequently, weaker X···X interactions for oxygen.

Among the $Cp_4Cr_4^{8+}$ FMO's, the three sets of Cp-centered, π-orbital blocks are represented as $a_1 + t_2$ (from the Cp a'_2 orbitals), $e + t_1 + t_2$ (from the Cp e''_1 orbitals), and $e + t_1 + t_2$ (from the Cp e''_2 orbitals). The bulk of the M–Cp bonding is contained in the first two sets although the high-energy set contains a small amount of metal character due to π back-bonding. Bonding capabilities of MCp fragments have been discussed elsewhere.[30]

The $Cp_4Cr_4^{8+}$ FMO's near the frontier region (−9 to −12 eV) are metal-centered according to reduced-charge analysis.[31] These metal FMO's are almost entirely comprised of d-orbital character (>95% of total metal character as determined from the orbital coefficients). Exceptions are the unfilled FMO's $2t_2$ (16% s + p), $2a_1$ (85% s + p), and $4t_2$ (75% s + p). These orbitals and s and p character are larger and better directed for M–X bonding than the others and will interact most strongly with the X_4^{8-} fragment. The 2e and $2t_1$ FMO's contain significant Cp character (ca. 25% of the orbital charge) and are M–Cp antibonding. The remaining FMO's, arranged from lowest to highest energy, are $1a_1$, $1t_2$, 1e, $1t_1$, and $3t_2$ and correspond to the $a_1 + e + t_2$ and $t_1 + t_2$ sets responsible for M–M bonding and antibonding, respectively, in the $Cp_4M_4^{8+}$ fragment.

The interaction of the $Cp_4Cr_4^{8+}$ and X_4^{8-} (X = O, S) fragments gives frontier regions that are in agreement with Dahl's symmetry-based model (boxed areas in Figures 4 and 5). In order of increasing energy, there is an occupied $1e + 1a_1 + 1t_2$ block of formal M–M bonding MO's with the empty $1t_1 + 2t_2$ block

(30) Elian, M.; Chen, M. M. L.; Mingos, D. M. P.; Hoffmann, R. *Inorg. Chem.* **1976**, *15*, 1148.

(31) Reduced charge Q_α on an atom in filled MO α is given by $Q_\alpha = 2\sum c_{i\alpha}\sum c_{j\alpha}S_{ij}$, where $c_{j\alpha}$ is summed over all atomic orbitals j and $c_{i\alpha}$ is summed over all the atomic orbitals i centered on the given atom.

Table VIII. Properties of Homonuclear M_4X_4 Cubane Clusters

compd	excess electrons	ideal symmetry	M–M dist, Å	formal bond order	magnetic moment, μ_B	ref
$Mo_4(\mu_3\text{-}O)_4O_4(OSPMe_2)_4$	4	D_{2d}	2 × 2.635 4 × 3.72	2		35
$Mo_4S_4(NC_6H_4Me)_4(S_2CNBu_2)_4$	4	D_{2d}	2 × 2.881 4 × 3.66	2	diamag	36
$Mo_4S_4(NC_6H_4Me)_4(S_2P(OEt)_2)_4$	4	D_{2d}	2 × 2.862 4 × 3.69	2	diamag	37
$V_4S_4R_4$ (R = Cp, Cp′)	8	T_d	2.87–2.88	6 × $^2/_3$	2.67–2.68	38, 39
$Mo_4S_4(S_2CNEt_2)_6$	10	D_{2d}	2 × 2.732 4 × 2.861	2 4 × $^3/_4$	paramag	40
$Mo_4S_4(i\text{-}PrCp)_4^{2+}$	10	T_d[a]	2.79–2.90	6 × $^5/_6$		12
$Mo_4S_4(edta)_2^{3-}$	11	D_{2d}	4 × 2.780 2 × 2.862	4 × 1 2 × $^3/_4$	2.0	41
$Mo_4S_4(i\text{-}PrCp)_4^{+}$	11	T_d[a]	2.86–2.92	6 × $^{11}/_{12}$	paramag	12
$Fe_4(CO)_4Cp_4^{+}$	11	T_d[a]	2.47–2.51	6 × $^{11}/_{12}$	2.2	42
$Cr_4O_4R_4$ (R = Cp, Cp′)	12	D_2	2 × 2.71 2 × 2.83 2 × 2.90	6	2.49 antiferromag	11, 28
$Cr_4S_4R_4$ (R = Cp, Cp′, Cp*)	12	T_d	2.82–2.85	6	diamag	7, 11, 13
$Mo_4S_4R_4$ (R = Cp, Cp′, Cp*, *i*-PrCp)	12	T_d	2.90	6	diamag	8, 12, 13, this work
$Mo_4S_4(CN)_8^{8-}$	12	T_d	2.85	6	diamag	26
$Fe_4(\mu_3\text{-}CO)_4Cp_4$	12	T_d	2.51–2.53	6	diamag	27
$Fe_4S_4(NO)_4$	12	T_d	2.64–2.66	6	weakly antiferromag	1, 10
$Fe_4S_4(NO)_4^{-}$	13	D_{2d}	4 × 2.688 2 × 2.703	4 × 1 2 × $^3/_4$	1.92	1
$Co_4(N\text{-}t\text{-}Bu)_4(NO)_4$	16	D_2	2 × 2.460 2 × 2.544 2 × 2.710	2 × 1 2 × $^3/_4$ 2 × $^1/_4$	diamag	43
$Fe_4S_4(S_2C_2(CF_3)_2)_4^{2-}$	18	D_{2d}	4 × 2.73 2 × 3.22	4 × $^3/_4$	diamag	44
$Fe_4S_4Cp^{2+}$	18	D_{2d}	4 × 2.834 2 × 3.254	4 × $^3/_4$	diamag	3
$Fe_4S_4Cp_4^{+}$	19	D_2	2 × 2.65 2 × 3.19 2 × 3.32	2 × 1 2 × $^1/_4$	paramag	45
$Mo_4S_4(CN)_8(NO)_4^{8-}$	20	D_{2d}	2 × 2.99	2		46
$Fe_4S_4Cp_4$	20	D_{2d}	2 × 2.650 4 × 3.67 4 × 3.36	2	diamag	47
$Co_4P_4Cp_4$	20	D_{2d}	2 × 2.504 4 × 3.63	2	diamag	48
$Co_4P_4(Cp^*)_4$	20	D_{2d}	2 × 2.65 4 × nonbond	2		49
$Co_4Sb_4(Cp)_4$	20	D_{2d}	2 × 2.66 4 × nonbond	2		49
$Co_4S_4Cp^{+}$	23	D_{2d}	4 × 3.17 2 × 3.33	4 × $^1/_8$	1.73	50
$Cr_4(OMe)_4(CO)_{12}^{4-}$	24	C_2	3.25–3.36	0	diamag	51
$Mo_4(OH)_4(CO)_8(NO)_4$	24	T_d	3.43	0	diamag	52
$W_4(OH)_4(CO)_{12}H_4$	24	T_d	3.48	0	diamag	53
$Re_4(OR)_4(CO)_{12}$ (R = H, Me)	24	T_d	3.48	0	diamag	54, 55
$Re_4(SMe)_4(CO)_{12}$	24	C_2	3.85–3.96	0	diamag	56
$Fe_4(AsMe)_4(CO)_{12}$	24	T_d	3.76	0	diamag	57
$Fe_4X_4(CO)_{12}$ (X = S, Se, Te)	24	T_d	3.44–3.48 (X = S)	0	diamag	58, 59
$Os_4O_4(CO)_{12}$	24	D_{2d}	3.19–3.25	0	diamag	60
$Co_4S_4Cp_4$	24	C_2	3.24–3.34	0	diamag	50
$Co_4Sb_4(CO)_{12}$	24	T_d	4.12	0	diamag	2
$Pt_4(OH)_4(CH_3)_{12}$	24	T_d	3.42	0	diamag	61, 6i
$Pt_4X_4(CH_3)_{12}$ (X = Cl, I)	24	T_d	nonbond	0	diamag	63, 64

[a] Distortion from T_d is slight and irregular.

of M–M antibonding MO's just above. In the Mo cluster the $1a_1$ MO lies *below* the 1e MO rather than vice versa for Cr. The energy levels calculated for $Cp_4Mo_4S_4$ are compared to the observed photoelectron spectrum (PES)[12] on the same (but displaced) energy scale in Figure 6. There is good agreement in the *relative* spacings of the a_1, e, and t_2 levels, but the calculated energies are about 4 eV too low. PES of the Cr clusters have not been reported.

The nature of the metal–ligand bonding in the $Cp_4M_4X_4$ clusters is not as simple as the Dahl model suggests. Much mixing between the formally M–Cp and M–X orbitals occurs. The formally M–Cp antibonding MO $3t_2$ contains 8.7% and 18.8% X_4 FMO character for X = O and S, respectively. M–X character is also found in the 12 M–M frontier orbitals, and a mild destabilization of these M–M orbitals results from the interaction with the X_4 FMO's. In contrast, Bottomley and Grein calculate a large, destabilizing interaction between the M–M frontier orbitals and X atom "lone pairs". It is this interaction that causes the $1a_1$ orbital to lie at high energy in their EHMO scheme.

In our calculations, the most obvious difference between the frontier regions of the oxide- or sulfide-capped cubanes is the relatively smaller HOMO–LUMO gap for the oxides: 0.46 vs. 1.10 eV for Cr_4O_4 vs. Cr_4S_4 and 0.60 vs. 1.18 eV for Mo_4O_4 vs. Mo_4S_4. Even though HOMO–LUMO energy separations calculated by the EHMO method are grossly inaccurate, the *trends* calculated for similar structures are usually reliable. We suggest that the antiferromagnetism[28] and distorted structure observed for $Cp_4Cr_4O_4$ is the result of the small HOMO–LUMO gap in this molecule.

Table IX. Frontier MO Wave Functions Expressed as Percent FMO Character

$Cp_4Cr_4O_4$ MO	O_4 FMO, %	Cp_4Cr_4 FMO, %
$2t_2$	11	50 ($3t_2$) + 15 ($2t_2$) + 24 ($1t_2$)
$1t_1$ (LUMO)	8	9 ($2t_1$) + 82 ($1t_1$)
$1t_2$ (HOMO)	7	39 ($3t_2$) + 3 ($2t_2$) + 51 ($1t_2$)
$1a_1$	7	6 ($2a_1$) + 87 ($1a_1$)
1e	0	2 (2e) + 98 (1e)
$Cp_4Cr_4S_4$ MO	S_4 FMO, %	Cp_4Cr_4FMO, %
$2t_2$	26	4 ($4t_2$) + 24 ($3t_2$) + 22 ($2t_2$) + 25 ($1t_2$)
$1t_1$ (LUMO)	14	24 ($2t_1$) + 60 ($1t_1$)
$1t_2$ (HOMO)	3	64 ($3t_2$) + 2 ($2t_2$) + 30 ($1t_2$)
$1a_1$	19	81 ($1a_1$)
1e	1	3 (2e) + 96 (1e)

Table X. Metal–Metal Overlap Populations in the $Cp_4M_4S_4$ Frontier Orbitals[a]

MO	$Cp_4Cr_4O_4$	$Cp_4Cr_4S_4$	$Cp_4Mo_4O_4$	$Cp_4Mo_4S_4$
$1t_2$	0.006	−0.010	0.053	−0.005
$1a_1$	0.195	0.258	0.283	0.362
1e	0.061	0.041	0.097	0.079

[a] Values represent summation over all individual M–M overlap populations within a given MO. Values for degenerate sets are for one component of the set.

A thermally accessible high-spin state is obviously consistent with a small HOMO–LUMO gap. The small gap also invites a second-order Jahn–Teller distortion. Mixing of the $^1A_1$ ($t_2^6t_1^0$) ground state with $T_2 \times T_1$ ($t_2^5t_1^1$) excited states is allowed via the e and t_2 vibrational modes.[32] Coupling to either of these modes could lead to a D_2 distortion. To date we have not performed EHMO calculations for distorted structures and thus cannot predict the magnitude of these distortions. The small HOMO–LUMO separation calculated for the as yet unknown $Cp_4Mo_4O_4$ cluster suggests that, when discovered, it too will be paramagnetic.

What factors are responsible for the different HOMO–LUMO gaps in the oxide and sulfide cubanes? In Table IX, the FMO contributions to the cubane frontier MO's are shown. For the most part, the admixture in the final MO of S_4 FMO character is greater than admixture of O_4 FMO character. This results from the fact that the M–S overlaps are greater than M–O overlaps (greater spatial extent of the S atomic orbitals) *and* the fact that the S orbitals better match the energy of the M–M FMO's. In other words, the more ionic M–O bonding is less effective than the more covalent M–S bonding in spreading the M–M manifold.

Other observations may be explained by these calculations. Dahl et al. have suggested that the $1t_1$ LUMO contains slight M–S antibonding character as evidenced by the small 0.014-Å increase in Fe–S distances upon reduction of the 12-electron cluster $Fe_4S_4(NO)_4$ to the monoanion. The 14% S_4 character in the LUMO of $Cp_4Cr_4S_4$ (Table IX) indicates significant M–S antibonding character in the $1t_1$ orbital.

The M–M overlap populations of the frontier orbitals (Table X) show some interesting facets. The qualitative Dahl model assigns an M–M bonding role to the $a_1 + e + t_2$ orbitals, such that if all these orbitals are filled, six M–M single bonds result. The overlap population analysis shows that *only* the $1a_1$ orbital is strongly metal–metal bonding. The 1e orbitals are weakly bonding. However, the HOMO, $1t_2$, is very weakly bonding in the oxides and is slightly *antibonding* in the sulfides. M–M antibonding character in the $1t_2$ orbital is consistent with the observed, slight M–M bond contraction as electrons are removed from the $1t_2$ orbital in the oxidation of $(i\text{-}PrC_5H_4)_4Mo_4S_4$.[12]

Table XI. Atomic Parameters Used in the EHMO Calculations

orbital		H_{ii}, eV	ζ	orbital		H_{ii}, eV	ζ
H	1s	−13.60	1.300	O	2s	−32.30	2.275
C	2s	−21.40	1.625		2p	−14.80	2.275
	2p	−11.40	1.625	S	3s	−20.00	1.817
					3p	−13.30	1.817

orbital		H_{ii}, eV	ζ_1	ζ_2	c_1[a]	c_2[a]
Cr	4s	−8.66	1.700			
	4p	−5.24	1.700			
	3d	−11.20	4.950	1.800	0.5058	0.6747
Mo	5s	−8.34	1.960			
	5p	−5.24	1.900			
	4d	−10.50	4.540	1.900	0.5899	0.5899

[a] Coefficients in the double-ζ expansion.

Table XII. Atomic Distances (Å) for EHMO Calculations

$Cp_4M_4X_4$	M–M	M–X	M–Cp(centroid)[a]
$Cp_4Cr_4O_4$	2.82	1.95	1.92
$Cp_4Cr_4S_4$	2.82	2.25	1.92
$Cp_4Mo_4O_4$	2.91	2.04	2.00
$Cp_4Mo_4S_4$	2.91	2.36	2.00

[a] C–C distances were 1.40 Å; C–H distances were 1.09 Å.

(32) Jotham, R. W.; Kettle, S. F. A. *Inorg. Chim. Acta* **1971**, *5*, 183.
(33) Ammeter, J. H.; Burgi, H.-B.; Thibeault, J. C.; Hoffmann, R. *J. Am. Chem. Soc.* **1978**, *100*, 3686.
(34) (a) Summerville, R. H.; Hoffmann, R. *J. Am. Chem. Soc.* **1976**, *98*, 7240. (b) Hoffmann, D. M.; Hoffmann, R. *J. Am. Chem. Soc.* **1982**, *104*, 3858.
(35) Mattes, R.; Mühlsiepen, K. *Z. Naturforsch., B: Anorg. Chem., Org. Chem.* **1980**, *35B*, 265.
(36) Wall, K.; Folting, K.; Huffman, J. C.; Wentworth, R. A. D. *Inorg. Chem.* **1983**, *22*, 2366.
(37) Wentworth, R. A. D.; Edelblut, A. W.; Folting, K.; Huffman, J. C. *J. Am. Chem. Soc.* **1981**, *103*, 1927.
(38) Eremenko, I. L.; Pasynskii, A. A.; Katugin, A. S.; Ellert, O. G.; Shklover, V. E.; Struchov, Y. T. *Izv. Akad. Nauk. SSSR, Ser.* Khim. **1984**, 1669; *Bull. Acad. Sci. USSR, Div. Chem. Sci. (Engl. Transl.)* **1984**, 1531.
(39) Bolinger, C. M. Ph.D. Thesis, University of Illinois, Champaign, IL, 1984.
(40) Mak, T. C. W.; Jasim, K. S.; Chieh, C. *Inorg. Chem.* **1985**, *24*, 1587.
(41) Shibahara, T.; Kuroya, H.; Matsumoto, K.; Ooi, S. *J. Am. Chem. Soc.* **1984**, *106*, 789.
(42) Trinh-Toan; Fehlhammer, W. P.; Dahl, L. F. *J. Am. Chem. Soc.* **1972**, *94*, 3389.
(43) Gall, R. S.; Connelly, N. G.; Dahl, L. F. *J. Am. Chem. Soc.* **1974**, *96*, 4017.
(44) Lemmen, T. H.; Kocal, J. A.; Lo, F. Y.-K.; Chen, M. W.; Dahl, L. F. *J. Am. Chem. Soc.* **1981**, *103*, 1932.
(45) Trinh-Toan; Fehlhammer, W. P.; Dahl, L. F. *J. Am. Chem. Soc.* **1977**, *99*, 402.
(46) Müller, A.; Eltzner, W.; Clegg, W.; Sheldrick, G. M. *Angew. Chem., Int. Ed. Engl.* **1982**, *21*, 536.
(47) Schunn, R. A.; Fritchie, C. J.; Prewitt, C. T. *Inorg. Chem.* **1966**, *5*, 892. Wei, C. H.; Wilkes, G. R.; Treichel, P. M.; Dahl, L. F. *Inorg. Chem* **1966**, *5*, 900.
(48) Simon, G. L.; Dahl, L. F. *J. Am. Chem. Soc.* **1973**, *95*, 2175.
(49) Johnson, R. E. Ph.D. Thesis, University of Wisconsin, Madison, WI, 1981.
(50) Simon, G. L.; Dahl, L. F. *J. Am. Chem. Soc.* **1973**, *95*, 2164.
(51) McNeese, T. J.; Cohen, M. B.; Foxman, B. M. *Organometallics* **1984**, *3*, 552.
(52) Albano, V.; Bellon, P.; Ciani, G.; Mannassero, M. *J. Chem. Soc., Chem. Commun.* **1969**, 1242.
(53) Albano, V.; Cianai, G.; Mannassero, M.; Sansori, M. *J. Organomet. Chem.* **1972**, *34*, 353.
(54) Nuber, B.; Oberdorfer, F.; Ziegler, M. L. *Acta Crystallogr., Sect. B: Struct. Crystallogr. Cryst. Chem.* **1981**, *B37*, 2062.
(55) Herberhold, M.; Süss, G.; Ellerman, J.; Gäbelein, H. *Chem. Ber.* **1978**, *111*, 2931.
(56) Harrison, W.; Marsh, W. C.; Trotter, J. *J. Chem. Soc., Dalton Trans.* **1972**, 1009.
(57) Röttinger, E.; Vahrenkamp, H. *J. Organomet. Chem.* **1981**, *213*, 1.
(58) Nelson, L. L.; Lo, F. Y.-K.; Rae, A. D.; Dahl, L. F. *J. Organomet. Chem.* **1982**, *225*, 309.
(59) Bogan, L. E.; Lesch, D. A.; Rauchfuss, T. B. *J. Organomet. Chem.* **1983**, *250*, 429.
(60) Bright, D. *J. Chem. Soc. D* **1970**, 1169.
(61) Preston, H. S.; Mills, J. C.; Kennard, C. H. L. *J. Organomet. Chem.* **1968**, *14*, 447.
(62) Spiro, T. G.; Templeton, D. H.; Zalkin, A. *Inorg. Chem.* **1968**, *7*, 2165.
(63) Rundle, R. E.; Sturdivant, J. K. *J. Am. Chem. Soc.* **1947**, *69*, 1561.
(64) Donnay, G.; Coleman, L. B.; Krieghoff, N. G.; Cowan, D. O. *Acta Crystallogr., Sect. B: Struct. Crystallogr. Cryst. Chem.* **1968**, *B24*, 157.

A $Cp_4M_4X_4$ cluster with only two excess electrons already has 45-80% of the metal-metal bonding afforded by the *frontier* orbitals. It is therefore not surprising to find a large number of clusters with fewer than 12 excess electrons but with fairly short M-M bonds (Table VIII). Another consequence of the nearly nonbonding or weakly antibonding nature of the $1t_2$ orbital is that first-order Jahn-Teller distortions for partially filled $1t_2$ configurations are expected to be relatively weak. Thus, idealized T_d and D_{2d} geometries with differences in M-M distances ≤ 0.13 Å are seen for electron configurations t_2^2-t_2^5 (8-11 excess electrons, Table VIII). Small distortions from T_d symmetry also imply small splittings of the degenerate levels so that complex magnetic behavior for clusters with 8-11 excess electrons is anticipated.

Conclusions

The preponderance of experimental observations supports the Dahl model rather than the bonding scheme proposed by Bottomley and Grein. The qualitative Dahl model is also supported by an EHMO calculation with the "standard" Hoffmann parameterization. The major differences between this parameterization and the one used by BG seems to be that the H_{ii} value used by BG for the metal s orbitals places them at much lower energies. The frontier M-M orbitals would then contain more metal s character, and this might account for the high energy BG find for the 1a MO. The paramagnetism of $Cp_4Cr_4O_4$ is suggested to be caused by the small HOMO-LUMO separation. Professor F. Bottomley has recently informed us that $Cp_4Cr_4O_4$ is *diamagnetic* below 20 K. This low-temperature diamagnetism is predicted by the model presented here. We thank Professor Bottomley for this information.[65]

The most convenient synthesis of Mo-S cubane clusters of the type $Cp'_2Cp''_2Mo_4(\mu_3\text{-}S)_4$ seems to be the reaction of $Cp'_2Mo_2(CO)_4$ (Mo≡Mo) with either $Cp''_2Mo_2S_2(SH)_2$ or $Cp''_2Mo_2(SC_3H_6S)_2$. These clusters are readily oxidized by two reversible 1e processes in acetonitrile—no reductions are observed in this solvent.

Acknowledgment. This work was supported by the National Science Foundation (Grant No. CHE-8305235). P.D.W. also thanks the donors of the Samuel H. Baer and Rackham Fellowships. We also thank Dr. W. M. Butler for assistance in the X-ray structure determinations.

Appendix: Details of the Calculations

Extended Hückel molecular orbital (EHMO) calculations were performed with use of the programs ICON8 and FMO furnished by R. Hoffmann. We have employed noniterative calculations with the weighted H_{ij} formula.[33] Slater orbitals were used, and double-ζ expansions were employed for the metal d orbitals. Atomic parameters are collected in Table XI.[34] Molecular geometry was idealized to T_d symmetry for the M_4X_4 core (D_{2d} with the Cp rings). Atomic distances are listed in Table XII. These distances were chosen to closely match X-ray structural results when applicable.

Supplementary Material Available: Table III (thermal factors) and Table VIIS (complete list of bond angles) (4 pages); Table XIIIS (listing of F_o vs. F_c) (15 pages). Ordering information is given on any current masthead page.

(65) Bottomley, F., unpublished results, 1986.

Contribution from the Institut de Chimie,
Université de Neuchâtel, CH-2000 Neuchâtel, Switzerland

Kinetics of Vanadium(III)-Chromium(II) Electron Transfer Revisited

François P. Rotzinger[1]

Received June 18, 1985

The oxidation of Cr^{2+} by V^{3+} has been reinvestigated at higher acidities. This has led to the observation of the previously unknown outer-sphere electron-transfer pathway (k_{OS}). At $[H^+] = 0.56$-2.56 M, 25 °C, and $I = 3.0$ ($NaClO_4$) the known rate law $-d[V^{3+}]/dt = -d[Cr^{2+}]/dt = k_{obsd}[V^{3+}][Cr^{2+}]$ was confirmed, but a different acid dependence, $k_{obsd} = k_{OS} + k_{IS}K_a/[H^+]$, was found. The rate constant $k_{IS} = 370 \pm 20$ M^{-1} s^{-1} for OH^--mediated inner-sphere electron transfer is in agreement with the previous studies, while $k_{OS} = 0.20 \pm 0.03$ M^{-1} s^{-1} is of the order of magnitude of the value predicted by the Marcus theory (0.01-0.08 M^{-1} s^{-1}). The (acid catalyzed) decomposition of the binuclear intermediate $VOHCr^{4+}$ was not detected at high $[H^+]$. The V^{3+}-Cr^{2+} reaction represents a d_{σ^*}-donor-d_π-acceptor system. The intrinsic rate advantage for inner-sphere electron transfer, $\chi = k_{IS}(K_{IS} \rightarrow 1)/k_{OS}(K_{OS} \rightarrow 1) > 12000$, is large and comparable with values found for d_{σ^*}-donor-d_{σ^*}-acceptor systems.

Introduction

The oxidation of Cr^{2+} by V^{3+} in acid aqueous solution was investigated and discussed by Espenson,[2] Sykes,[3] Haim,[4] and Adin and Sykes.[5] The presently accepted mechanism involves reactions 1-3 with $k_{IS}K_a = 0.624$ s^{-1} and $k_{-IS}/k_H = 0.108$ M.[2,6] The

$$V^{3+} + H_2O \rightleftarrows VOH^{2+} + H^+ \quad K_a \tag{1}$$

$$VOH^{2+} + Cr^{2+} \rightleftarrows VOHCr^{4+} \quad k_{IS}, k_{-IS} \tag{2}$$

$$VOHCr^{4+} + H^+ \rightarrow V^{2+} + Cr^{3+} + H_2O \quad k_H \tag{3}$$

$$V^{3+} + Cr^{2+} \rightarrow V^{2+} + Cr^{3+} \quad k_{OS} \tag{4}$$

relatively inert binuclear intermediate $VOHCr^{4+}$ with d^3-d^3 electron configuration is present at steady-state concentration. It is formed via inner-sphere electron transfer (reaction 2) and decays via acid catalysis (reaction 3). The outer-sphere reaction (4), however, was not detected under the experimental conditions ($[H^+] \leq 0.5$ M) used in earlier studies.[2,5] Therefore, the reaction was reinvestigated at higher acidity ($[H^+] = 0.56$-2.56 M, $I = 3.0$), where the concentration of the very reactive VOH^{2+} is lower. Then, the contribution of the outer-sphere reaction (4) became detectable.

The V^{3+}-Cr^{2+} reaction represents a d_{σ^*}-donor-d_π-acceptor electron-transfer system (d_{xy}, d_{xz}, and d_{yz} with π symmetry and $d_{x^2-y^2}$ and d_{z^2} with σ symmetry with respect to the metal-ligand bond axis). The intrinsic rate advantage for the inner-sphere pathway is of interest in comparison with the previously studied d_{σ^*}-donor-d_{σ^*}-acceptor systems.[7-9] In the d_{σ^*}-d_{σ^*} and d_{σ^*}-d_π systems, efficient donor-acceptor overlap is possible, since

(1) Present address: Institut de Chimie Physique, Ecole Polytechnique Fédérale, CH-1015 Lausanne, Switzerland.
(2) Espenson, J. H. *Inorg. Chem.* **1965**, *4*, 1025.
(3) Sykes, A. G. *Chem. Commun.* **1965**, 442.
(4) Haim, A. *Inorg. Chem.* **1966**, *5*, 2081.
(5) Adin, A.; Sykes, A. G. *J. Chem. Soc. A* **1968**, 351.
(6) Haim, A. *Prog. Inorg. Chem.* **1983**, *30*, 273.
(7) Rotzinger, F. P.; Kumar, K.; Endicott, J. F. *Inorg. Chem.* **1982**, *21*, 4111.
(8) Endicott, J. F.; Kumar, K.; Ramasami, T.; Rotzinger, F. P. *Prog. Inorg. Chem.* **1983**, *30*, 141.
(9) Kumar, K.; Rotzinger, F. P.; Endicott, J. F. *J. Am. Chem. Soc.* **1983**, *105*, 7064.

0020-1669/86/1325-4570$01.50/0